

Toward an Understanding of the Pressure Effect on the Intramolecular Vibrational Frequencies of Sulfur Hexafluoride

Matteo Boccalini, Roberto Cammi,* Marco Pagliai,* Gianni Cardini,* and Vincenzo Schettino



Cite This: *J. Phys. Chem. A* 2021, 125, 6362–6373



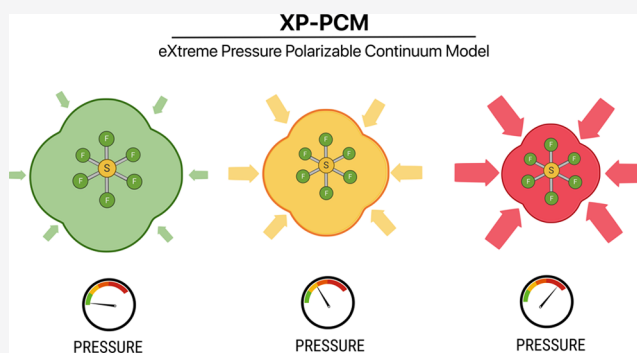
Read Online

ACCESS |

Metrics & More

Article Recommendations

ABSTRACT: The structural and vibrational properties of the molecular units of sulfur hexafluoride crystal as a function of pressure have been studied by the Extreme Pressure Polarizable Continuum Model (XP-PCM) method. Within the XP-PCM model, single molecule calculations allow a consistent interpretation of the experimental measurements when considering the effect of pressure on both the molecular structure and the vibrational normal modes. This peculiar aspect of XP-PCM provides a detailed description of the electronic origin of normal modes variations with pressure, via the curvature of the potential energy surface and via the anharmonicity of the normal modes. When applied to the vibrational properties of the sulfur hexafluoride crystal, the XP-PCM method reveals a hitherto unknown interpretation of the effects of the pressure on the vibrational normal modes of the molecular units of this crystal.



INTRODUCTION

The study of structural and dynamic properties of both liquid and solid materials at high pressure, mainly carried out in the diamond anvil cell (DAC),^{1–3} is an active research field^{1,2,4–7} for its implication in both applied science and technology and knowledge of atomic and molecular properties. Indeed, in a recent paper by Cammi, Rahm, Hoffmann and Ashcroft⁸ it has been envisaged that basic electronic properties along the periodic table (like atomic electronic configuration and electronegativity) exhibit drastic changes at high pressures thus modulating general chemical behaviors.

In particular, in studying molecular crystals at high pressures, the general properties can be conveniently investigated with vibrational spectroscopy and some experimental findings can be achieved by comparison with computational models. A general approach to model molecular crystals involves periodic systems.^{9–12} Accurate determination of structural and spectroscopic properties by *ab initio* solid state calculations requires elevated computational resources.^{10,11} But, even when vibrational properties are obtained either by *ab initio* molecular dynamics simulations or by crystal calculations in the harmonic approximation^{10–12} subsequent extraction of high pressure effects on single molecule is not an easy task.

The recently introduced eXtreme Pressure Polarizable Continuum Model (XP-PCM)^{4,13–18} allows for *ab initio* calculations at high pressure on a single molecular unit of the system of interest at a reduced computational cost. In the XP-PCM calculations the main pressure effects on the vibrational properties can be easily taken into account and

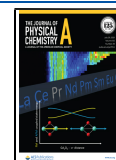
these are interpreted in terms of curvature and anharmonicity of the potential energy surface, providing useful insights on pressure effects on the intramolecular normal modes,^{16–18} a kind of analysis which is not currently available in periodic calculations. In the XP-PCM approach the interactions with the environment are modeled using the Polarizable Continuum Model (PCM),^{19,20} properly taking into account the pressure effect by increasing the Pauli repulsion due to the external medium on the molecule.⁴ This tuning of the pressure is obtained by reducing the volume of the cavity hosting the molecular unit.^{4,13,16,17,21}

In the present paper the XP-PCM method has been applied to study the vibrational frequencies of sulfur hexafluoride (SF₆) as a function of the pressure and how these effects can be properly analyzed. Sulfur hexafluoride is an interesting candidate, since the molecular structure of isolated SF₆, as depicted in Figure 1, has a perfect octahedral arrangement (almost spherical). The high symmetry of the SF₆ molecule (O_h) and the limited number of atoms allow to analyze the effect of pressure on vibrational properties at high level of theory and to compare the results with the available

Received: March 23, 2021

Revised: June 17, 2021

Published: July 15, 2021



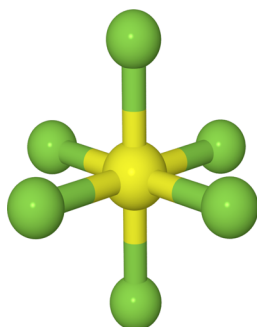


Figure 1. Molecular structure of sulfur hexafluoride SF₆.

experimental measurements.^{22,23} In fact, several IR and Raman experiments^{22–26} are available on the molecular crystal for different phases both at ambient and high pressures.^{23,26}

The article is organized as follows. First, the XP-PCM theory is briefly reviewed in the “XP-PCM Theory” section, then the phase diagram is discussed in the “Phase Diagram of Sulfur Hexafluoride” section. The computational procedure is described in the “Computational Protocol and Details” section and finally the results of the calculations are presented in the “Results and Discussion” section, where a detailed analysis of the vibrational properties in terms of curvature and relaxation contributions are discussed. Final remarks are reported in the “Conclusions” section.

METHODS

XP-PCM Theory. Let us consider a molecular systems embedded in the external medium of the XP-PCM model. The electronic energy determining its potential energy surface is given by eq 1

$$G_{er} = \left\langle \Psi \left| \hat{H}^0 + \frac{1}{2} \bar{\mathbf{Q}}(\Psi) \cdot \hat{\mathbf{V}} + \hat{\mathbf{V}}_r \right| \Psi \right\rangle + \tilde{V}_{nn} \quad (1)$$

where \tilde{V}_{nn} is the nuclei–nuclei interaction contribution in the presence of the external medium, $\bar{\mathbf{Q}}(\Psi) \cdot \hat{\mathbf{V}}$ is the PCM electrostatic interaction term²⁰ and $\hat{\mathbf{V}}_r$ is the Pauli repulsion term, which describes the exchange–repulsion contribution due to the overlap of the electron distribution of the studied molecular system with the mean electron distribution of the external medium (modeled by an uniform distribution outside the cavity following the PCM approach^{19,20}). The repulsion term is expressed by eq 2

$$\hat{\mathbf{V}}_r = \int \hat{\rho}(\mathbf{r}) \mathcal{R}(\mathbf{r}) \, d\mathbf{r} \quad (2)$$

where $\hat{\rho}(\mathbf{r}) = \sum_i^n \delta(\mathbf{r} - \mathbf{r}_i)$ is the electron density operator (over the n electrons of the molecular system).

\mathcal{R} is a factor representing a step barrier potential located at the boundary of the molecular cavity, as reported in eq 3:

$$\mathcal{R}(\mathbf{r}) = \mathcal{Z} \Theta_C(\mathbf{r}) \quad \Theta_C(\mathbf{r}) = \begin{cases} 0 & \mathbf{r} \in D_C \\ 1 & \mathbf{r} \notin D_C \end{cases} \quad (3)$$

where \mathcal{Z} is the height of the potential barrier and $\Theta_C(\mathbf{r})$ is a generalized Heaviside step function with a value equal to zero inside the cavity and equal to one outside of it (D_C denotes the domain of the physical space inside the cavity). The height of the potential barrier \mathcal{Z} depends on the volume of the cavity, V_c ⁴ as shown in eq 4:

$$\mathcal{Z} = \mathcal{Z}_0 \left(\frac{V_c}{V_c^0} \right)^{-\frac{3+N}{3}} \quad (4)$$

where \mathcal{Z}_0 is the height corresponding to a reference upper value of the cavity volume, V_c^0 , and N is a semiempirical parameter that gauges the strength of the Pauli repulsive barrier originated from the external medium, and which can be estimated by comparison of the computed pressure–volume results of XP-PCM with the available experimental pressure–volume data as expressed by Murnaghan equation²⁷ for different phases. The height of the potential barrier \mathcal{Z} given in eq 4 implicitly accounts for the pressure dependence of the properties of the external medium¹³ (i.e., the dielectric permittivity and average electron density).

The pressure p is computed as the negative of the derivative of the electronic energy, eq 5, with respect to the cavity volume V_c at constant number of particles n :

$$p = - \left(\frac{\partial G_{er}}{\partial V_c} \right)_n \quad (5)$$

The cavity is defined in terms of overlapping spheres centered on the atomic nuclei with radius related, by a uniform scaling factor (f), to the corresponding atomic van der Waals radii (R_{vdW}^i).²⁸ The cavity volume may be freely reduced by decreasing the scaling factor with respect to the reference value $f^0 = 1.2$.^{8,13,16–18} It has been recently shown²⁹ that the XP-PCM model is able to faithfully reduce the van der Waals radii of elements in agreement with available experimental data, suggesting that the same procedure can be successfully extended in studying molecular species.

The Pauli repulsion potential depends indirectly on f . In fact, the repulsion potential is related both to the numeral density of the external medium $n_s(f) = n_s^0 \left(\frac{f^0}{f} \right)^3$ and by a semiempirical

parameter $\gamma_N(f) = \frac{4\pi}{0.7E_h a_0^3} \left(\frac{f^0}{f} \right)^N$, with $3 \leq N \leq 6$, which can be experimentally determined, where a_0 and E_h are conversion factors from Bohr and Hartree, respectively.

The equilibrium geometries of the molecule under pressure correspond to the minimum of the potential energy surface determined by the electronic functional G_{er} of eq 1.

The vibrational harmonic frequencies are obtained from the Hessian matrix of the second derivatives of G_{er} with respect to the atomic displacements obtained numerically by the gradients.

As mentioned in the Introduction, the XP-PCM helps to achieve relevant insights on the pressure effect on vibrational frequencies by a partition in curvature and relaxation (or anharmonicity) contributions;^{4,16,17} these contributions are referred to also as direct and indirect effects, respectively.

The Effect of the Pressure on the Equilibrium Geometry and Vibrational Frequencies and Its Direct and Indirect Contributions. Describing the molecule as a set of harmonic oscillators, the electronic energy G_{er} in eq 5 can be expanded as a function of the vibrational normal mode coordinates of the isolated molecule \mathbf{Q} and of the pressure p , as shown in the Taylor expansion in eq 6:

$$G_{er}(\mathbf{Q}, p) = G_{er}(\mathbf{Q}, 0) + p \sum_i \Gamma_i Q_i + p \sum_i \Gamma_{ii} Q_i^2 + \dots \quad (6)$$

where $G_{er}(\mathbf{Q}, 0)$ is the electronic energy at zero pressure (i.e., that of the isolated molecule), as a function of the normal coordinates \mathbf{Q} ; Γ_i and Γ_{ii} are partial derivatives of G_{er} and their physical meaning is summarized in the following.

Equation 7 shows that Γ_i is the mixed second order derivative:

$$\Gamma_i = \left(\frac{\partial^2 G_{er}}{\partial p \partial Q_i} \right)_{\mathbf{Q}=0} = \left(\frac{\partial G_{er}^{Q_i}}{\partial p} \right)_{\mathbf{Q}=0} \quad (7)$$

and it represents the direct effect of pressure on the forces on the nuclei along the normal coordinate Q_i . Due to the isotropic pressure, Γ_i is forced to be different from zero only for totally symmetric (TS) normal mode coordinates. In particular, the variations of the equilibrium geometry along the TS normal coordinates $\{Q_i^{TS}\}$ are given by eq 8

$$Q_i^{eq}(p) = -\frac{\Gamma_i}{k_i} p \quad i \in \{Q_i^{TS}\} \quad (8)$$

where k_i is the harmonic force constants of the i^{th} normal mode. Equation 8 shows also how the pressure affects the geometry not only through the coupling coefficients $\{\Gamma_i\}$ but also with the normal mode force constants, $\{k_i\}$, which describe the stiffness of the normal modes.

The Γ_{ii} is expressed in eq 9 by the mixed third-order coefficient:

$$\Gamma_{ii} = \left(\frac{\partial^3 G_{er}}{\partial p \partial^2 Q_i} \right)_{\mathbf{Q}=0} = \left(\frac{\partial k_i}{\partial p} \right)_{\mathbf{Q}=0} \quad (9)$$

and it represents the direct effect of the pressure on the force constant k_i of the i^{th} normal mode. Γ_{ii} could be different from zero for any vibrational normal mode.

The total effect of pressure on the vibrational harmonic force constants is given by eq 10:

$$\tilde{k}_i(p) = k_i + p \left(\Gamma_{ii} - \sum_j^{TS} \frac{g_{ij} \Gamma_j}{k_j} \right) \quad (10)$$

where g_{ij} is the cubic anharmonic constant coupling the normal mode i with a totally symmetric normal mode j .

Furthermore, the effect of the pressure on the vibrational frequencies can be partitioned into a curvature (direct) and a relaxation (indirect) contribution,^{4,13,16,17} as shown in eq 11:

$$\left(\frac{\partial \nu(p)}{\partial p} \right)_{\mathbf{Q}(p)} = \left(\frac{\partial \nu(p)}{\partial p} \right)_{cur} + \left(\frac{\partial \nu(p)}{\partial p} \right)_{rel} \quad (11)$$

with

$$\left(\frac{\partial \nu(p)}{\partial p} \right)_{cur} = \left(\frac{\partial \nu(p)}{\partial p} \right)_{\mathbf{Q}(0)} \quad (12)$$

$$\left(\frac{\partial \nu_i(p)}{\partial p} \right)_{rel} = \left(- \sum_j^{TS} \tilde{g}_{ij}(0) \frac{\Gamma_j}{k_j(0)} \right)_{\mathbf{Q}(0)} \quad (13)$$

where $\nu(p)$ denotes the vibrational frequencies evaluated at the equilibrium geometries and $\mathbf{Q}(0)$ the equilibrium geometry of the isolated molecule.

From eqs 11–13, the pressure effect on the harmonic force constants can be partitioned in a *curvature (or direct)* effect,

represented by Γ_{ii} which relates the influence of pressure to changes in the electron density of the system, and a *relaxation (or indirect)* effect, involving the cubic anharmonicities g_{ij} , which is related to the pressure induced modification of the equilibrium geometry of the molecular system.

Equations 11–13 are of fundamental importance to analyze the effect of pressure on vibrational properties of molecules in the crystal. In essence, the *curvature* contribution, due to the variation of the second derivative of the potential energy surface, accounts for the confinement effect due to the repulsive intermolecular interactions, evaluated at the zero-pressure equilibrium geometry, while the *relaxation* contribution is related to the variation of the equilibrium geometry of the molecule through the anharmonic force constants. In more general terms, this analysis is motivated by the need to give answer to some questions like “Why do the molecules respond to the pressure in the way observed? Why does this response depend on the various vibrational normal modes? Is there a property of the normal modes that governs their response to the pressure?”. We remark that a similar partitioning, useful to rationalize observed frequency shifts with pressure, has previously been carried out with a semiclassical approach by Moroni et al.³⁰ The XP-PCM method has the definite advantage of accurately estimating the two contributions for a general molecular system.

■ PHASE DIAGRAM OF SULFUR HEXAFLUORIDE

The phase diagram of SF_6 has been studied as a function of both temperature and pressure. At ambient pressure it has been found by neutron diffraction experiments³¹ that at 94.3 K a phase transition occurs from a high temperature orientationally disordered structure (space group $Im\bar{3}m$, $Z = 2$) to a monoclinic structure (space group $C_2/m - C_{2h}^3$ with $Z = 6$). The molecules are found in two different sites, with site symmetry $2/m$ (or C_{2h}) or m (or C_s). The reduction of molecular symmetry and the intermolecular interactions in the crystal produce a multiplet structure in the vibrational spectra. The correlation diagram for the C_{2h} site shows that the degeneracy of the normal modes is removed. Therefore, for molecules on this site it is expected that the A_{1g} , E_g , and T_{2g} should appear as singlet, doublet, and triplet, respectively, in the Raman spectrum. The same turns out to be the case for the two molecules on the C_s site since an additional Davydov component is only infrared active. For this latter lattice site each component of the infrared modes should become Raman active. In the Raman spectrum of Salvi and Schettino²² the A_{1g} mode shows two components which should be taken as arising from the C_{2h} and C_s sites. For the E_g and T_{2g} modes 4 and 3 components are observed, respectively, and could, by analogy, be taken as arising from the molecules on different sites. No evidence is found of Raman activation of the infrared modes or of infrared activation of the Raman modes. This implies that in the low temperature phase the molecular deformation of the SF_6 octahedra is actually very small. The model used in the present paper appears, therefore, suited for the system under study. As a whole the internal Raman active components should classify as $14 A_g \oplus 7 B_g$ in the factor group.

The SF_6 phase diagram as a function of pressure has been explored by X-ray diffraction up to 32 GPa.²³ A phase transition to the same crystal structure of the low temperature phase described by Cockcroft and Fitch³¹ has been observed at 2 GPa (phase II). Further transitions have been observed to occur at 12 GPa (phase III) and 24 GPa (phase IV) as

evidenced by the appearance of new lines in the diffraction pattern and changes in the Raman spectrum. It can be remarked that the multiplet structure observed in phase III is identical with that reported by Salvi and Schettino at low temperature and ambient pressure,²² apart from the improved resolution of the low temperature spectrum. It can be argued that also at high pressure deviations from the octahedral structure of the SF₆ units are very small. Therefore, a geometry belonging to the *O_h* point group symmetry^{32–35} has been adopted in the initial configuration of DFT calculations. Subsequently, the pressure effects on both the structural and vibrational properties of SF₆ have been simulated by increasing the Pauli exchange repulsion experienced by the target molecule properly reducing the cavity volume using the XP-PCM method.^{4,13,16–18}

Computational Protocol and Details. All the calculations have been performed in the DFT framework adopting the 6-311G(d)³⁶ basis set with a modified version of the Gaussian 09 rev.C.01 suite of programs.³⁷ The exchange–correlation energy functional has been selected by verifying the accuracy in reproducing the experimental S–F bond length with some exchange and correlation functionals.

The bond length of the optimized SF₆ molecule (in gas phase) obtained with the selected exchange and correlation functional is reported in Table 1; the computed bond lengths are in the range between 1.588 Å (PBE0 and WB97XD) and 1.638 Å (BLYP).

Table 1. Bond Length (Å) of Isolated SF₆ Molecule for Selected Exchange and Correlation Functionals, Using the 6-311G(d) Basis Set^a

functional	S–F (Å)
exp ³⁸	1.561
SVWN ^{39–42}	1.591
BLYP ^{43,44}	1.638
B3LYP ^{44,45}	1.603
CAM-B3LYP ⁴⁶	1.589
O3LYP ⁴⁷	1.600
PBE ^{48,49}	1.622
PBE0 ⁵⁰	1.588
WB97XD ⁵¹	1.588

^aThe computed SF₆ bond length is compared with experimental data in the gas phase.³⁸

PBE0 and WB97XD provide results in better agreement with experiments.³⁸ Therefore, we have decided to report the structural and spectroscopic analysis on the basis of

calculations with the PBE0 functional, unless otherwise specified.

The XP-PCM protocol is the same employed with success in the studies on P₄S₃¹⁷ and on As₄S₄.¹⁸ Argon has been used as solvent, while van der Waals radius for S and F have been set to 1.80 and 1.47 Å, respectively.²⁸ The scaling factor *f* has been varied between 1.2 and 0.975, allowing to study the system in the pressure range between 0 and 10.2 GPa for *N* = 3 and between 0.0 and 24.6 GPa for *N* = 6, respectively. To ensure a smooth behavior of electronic and structural properties with pressure, the molecular cavities have been described using tesserae with an average size of 0.05 Å² (the value has been imposed with the keyword TSARE and it is about an order of magnitude lower than the default value which is 0.2 Å²). However, it has been verified that a value of 0.075 Å² represents a good compromise between accuracy and computational time for the present calculations.

Analogously to XP-PCM studies on P₄S₃¹⁷ and As₄S₄,¹⁸ the protocol consists in a molecular geometry optimization performed with a self-consistent procedure until the structure convergence is reached for each scaling factor *f* (i.e., pressure value). Once the equilibrium geometry has been located, the procedure is repeated for a new cavity with a smaller scaling factor. The convergence criteria imposed in the calculations are *Maximum force* lower than 2×10^{-6} E_h/a₀, *RMS force* lower than 1×10^{-6} E_h/a₀, *Maximum atomic displacement* lower than 6×10^{-6} a₀ and *RMS atomic displacement* lower than 4×10^{-6} a₀. An ultrafine grid has been adopted for the evaluation of the numerical integrals. All the calculations on SF₆ have been performed with values for the *N* parameter equal to both 3 and 6, as discussed in the following. This choice of using the limiting values for *N* is based on previous works^{4,13,15–17,52} on XP-PCM that proved how it was possible to interpret the experimental observable with pressure. No fitting procedures have been carried out to further improve the agreement between experimental and computed data.

The harmonic vibrational frequency calculation has been carried out for all the optimized geometries. The pressure effects on vibrational normal modes have been analyzed to determine both the *curvature* and *relaxation* contributions. The *curvature* contribution, eq 12, has been evaluated through the calculation of the vibrational frequencies, obtained by numerical differentiation, as a function of pressure at fixed equilibrium geometry *in vacuo*. The *relaxation* contribution can be evaluated numerically by eq 11 or analytically by determining the derivative of frequency variation with pressure as in eq 13.

Table 2. Normal Modes (cm^{−1}) of SF₆^a

symm	NM	scaled	exp ^b	Δν	%	free	assignment
T _{2u}	328.2	346.9	(345.7) ^c	1.2	0.3	326.9	ν ₆ , antisymm degenerate bending
T _{2g}	489.6	517.5	523.5	6	1.2	488.7	ν ₅ , symm degenerate bending
T _{1u}	578.3	611.3	(611)	0.3	0.05	578.9	ν ₄ , antisymm degenerate bending
E _g	626.7	662.4	644	18.4	2.9	627.1	ν ₂ , symm degenerate stretching
A _{1g}	729.6	771.2	775	3.8	0.5	728.0	ν ₁ , symm stretching
T _{1u}	925.7	978.4	(936)	42.4	4.5	934.2	ν ₃ , antisymm degenerate stretching

^aXP-PCM results with *f* = 1.20 at the PBE0/6-311G(d) level of theory. TSARE = 0.05. Vibrational frequencies (NM) have been scaled by a factor of 1.057, obtained through a fitting procedure for the calculated frequencies of the isolated molecule (without XP-PCM). ^bP.R. Salvi and V. Schettino.²² ^cThis frequency has been obtained from the analysis of combination bands. Δν represents the absolute error in cm^{−1}, while with % are reported the absolute error in percentage. The assignment has been taken from Herzberg.⁵³ Symmetries for the “free” molecule calculated frequencies at the same XP-PCM level of theory are reported.

RESULTS AND DISCUSSION

IR and Raman Spectra at Ambient Pressure. The isolated SF₆ molecule belongs to the O_h point group and

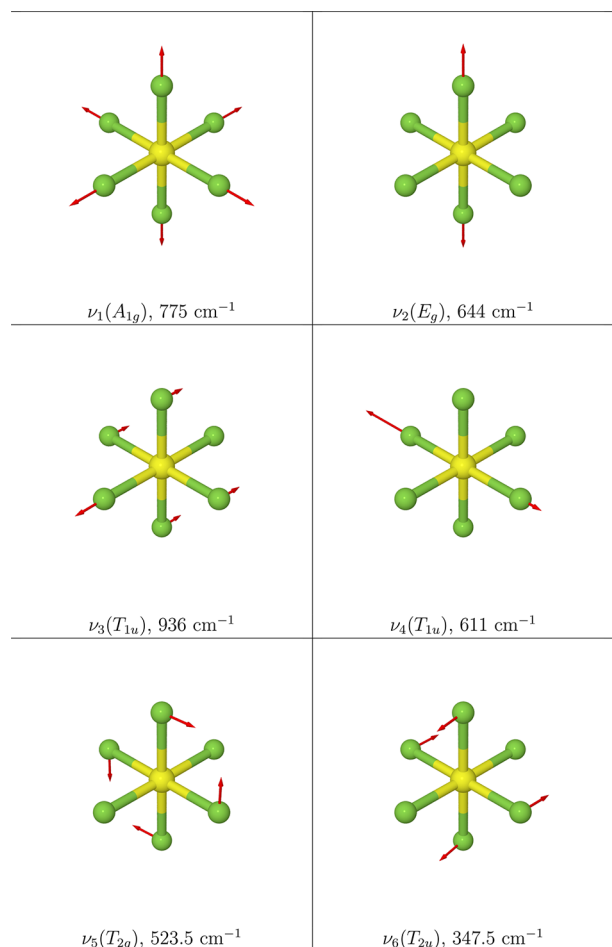


Figure 2. Graphical representation of the normal modes of SF₆ with the assignment proposed by Salvi et al.²² Only one component of the each degenerate modes is shown.

Table 3. Comparison of K_0 and K_p Murnaghan Parameters Obtained by XP-PCM Calculations on SF₆ and Experiments²³

	$N = 3$	$N = 6$	exp phase I	exp phase II
K_0	6.46	7.79	6.3(2)	8.5(8)
K_p	5.01	7.19	4	7.4(9)

consequently the vibrational normal modes can be grouped in the irreducible representations as

$$\Gamma = A_{1g} \oplus E_g \oplus T_{2g} \oplus 2T_{1u} \oplus T_{2u} \quad (14)$$

The normal modes with symmetry A_{1g} , E_g , and T_{2g} are Raman active, whereas the two T_{1u} modes are IR active. The normal mode of T_{2u} symmetry is both IR and Raman inactive, but it has been identified and assigned by Salvi et al.²² analyzing combination bands in the IR spectrum of the crystal.

Calculated and experimental frequencies are compared in Table 2. It can be noted that the scaled calculated frequencies agree quite satisfactorily with the crystal frequencies.^{22,23} This may imply that the XP-PCM approach somehow accounts for the static field acting on the molecule albeit not (obviously) for

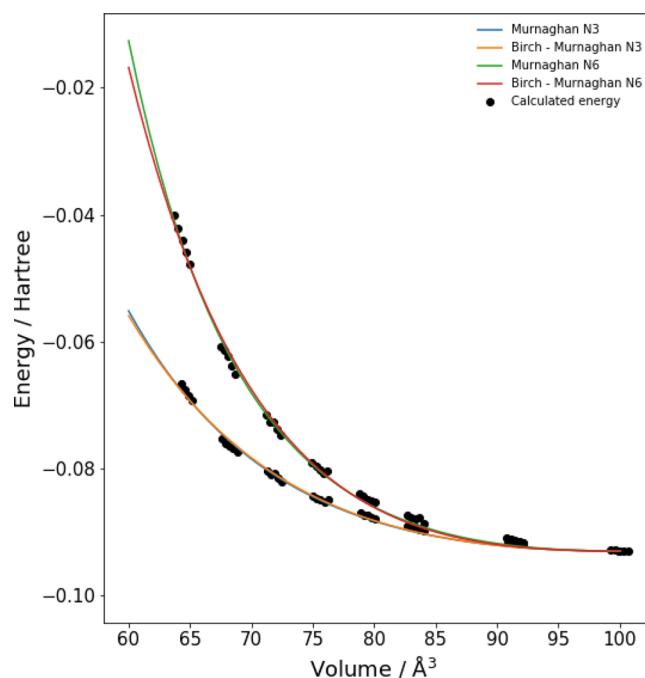


Figure 3. Fit of energy values with both Murnaghan²⁷ and Birch–Murnaghan⁵⁶ equations of state. The procedure has been carried out for XP-PCM calculations with both $N = 3$ and $N = 6$.

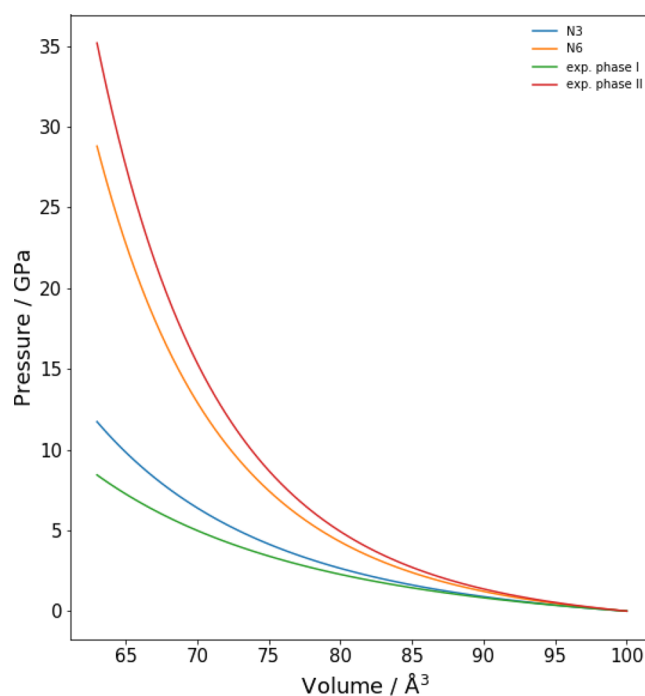


Figure 4. Comparison between experimental and computed Murnaghan²⁷ equation of states with volume. Cavity volume and molecular volume have been adopted for calculations and experiments, respectively.

the intermolecular coupling giving rise to the Davydov splitting.

The vibrational assignment is that reported by Herzberg⁵³ and confirmed in several studies of the vibrational properties of SF₆.^{22–26,54,55} In particular, the three lower vibrational frequencies are bending normal modes, whereas the others are stretching modes.

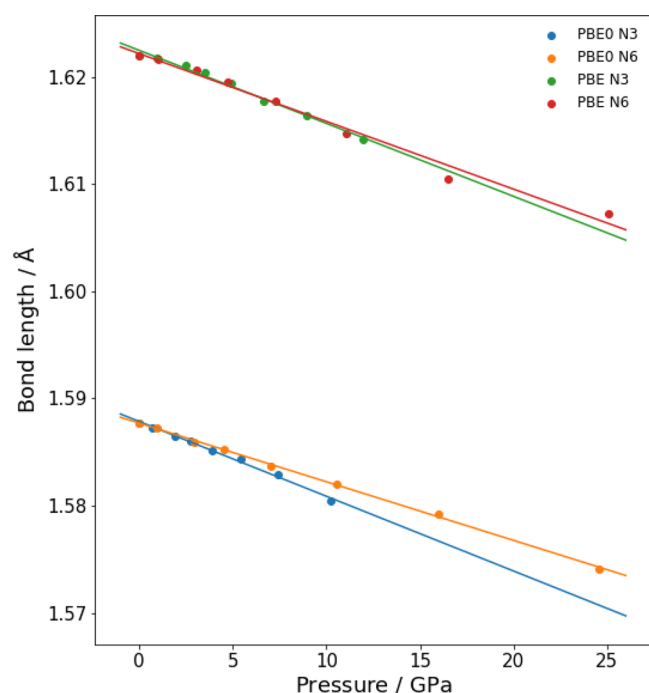


Figure 5. S–F bond length (in Å) with the pressure (in GPa). The results are reported for both PBE and PBE0 exchange and correlation functionals in conjunction with 6-311G(d) basis set. The equations of linear regression are PBE N3, $y = -0.00068x + 1.62246$; PBE N6, $y = -0.00063x + 1.62216$; PBE0 N3, $y = -0.00070x + 1.58786$; and PBE0 N6, $y = -0.00055x + 1.58770$.

Table 4. Pressure Coupling Constant Γ_i ($E_h a_0^{-1} \text{ GPa}^{-1}$), Defined in Eq 7, Harmonic Force Constant in the Gas Phase k_i ($E_h a_0^{-2}$), Ratio Γ_i/k_i (\AA GPa^{-1}), and Pressure Coefficient dQ_i/dp (\AA GPa^{-1}) of SF_6

	Γ_i	k_i	$-\frac{\Gamma_i}{k_i}$	$\frac{dQ_i^{\text{eq}}}{dp}$
$N = 3$	0.00123	0.7201	−0.00173	−0.00171
$N = 6$	0.00099	0.7201	−0.00137	−0.00134

A graphical representation of the normal modes is reported in Figure 2.

Structural Properties. The first information on the response to pressure of SF_6 molecule has been achieved by computing the Murnaghan²⁷ and Birch–Murnaghan⁵⁶ equation of state and comparing the results with experimental data.²³

The relation between the scaling factor f and the pressure can be obtained assuming that the cavity volume can be initially described through the Murnaghan equation:²⁷

$$P(V) = \frac{K_0}{K_p} \left[\left(\frac{V_0}{V(f)} \right)^{K_p} - 1 \right] \quad (15)$$

in which V_0 is the cavity volume for $f = 1.20$ and $V(f)$ is the cavity volume for a certain scaling factor, whereas $K_0 = -V \left(\frac{\partial p}{\partial V} \right)_{p=0}$ and $K_p = \left(\frac{\partial K_0}{\partial p} \right)_{p=0}$.

The K_0 and K_p parameters are obtained by using a fitting procedure of the electronic energy functional:

$$G_{\text{er}}(V) = \frac{K_0}{K_p} \cdot V(f) \cdot \left[\left(\frac{V_0}{V(f)} \right)^{K_p} \cdot \left(\frac{1}{(K_p - 1)} \right) + 1 \right] - \frac{K_0 V_0}{K_p - 1} \quad (16)$$

A similar procedure has been performed using the Birch–Murnaghan equation of state:⁵⁶

$$P(V) = \frac{3K_0}{2} \left[\left(\frac{V_0}{V} \right)^{7/3} - \left(\frac{V_0}{V} \right)^{5/3} \right] \times \left\{ 1 + \frac{3}{4}(K_p - 4) \left[\left(\frac{V_0}{V} \right)^{2/3} - 1 \right] \right\} \quad (17)$$

The values of both the K_0 and K_p Murnaghan parameters obtained by XP-PCM calculations are compared in Table 3 with experimental data by Rademacher et al.²³ for both phase I and phase II. The XP-PCM calculations have been carried out with the N parameter equal to both 3 and 6. The Birch–Murnaghan equation of state obtained for phase II by Rademacher et al.²³ with periodic DFT calculations (PBE + TS) provides results in excellent agreement with experiments.

The comparison of the fitting procedure with both the Murnaghan²⁷ and Birch–Murnaghan⁵⁶ equations of state is reported in Figure 3. It is possible to appreciate from the Figure 3 that the curves of the energy as function of the cavity volume are accurately reproduced with both the Murnaghan²⁷ and Birch–Murnaghan⁵⁶ equations of state, with appreciable differences only outside the range of the computed data (cavity volume $< 65 \text{ \AA}^3$).

The fitting procedure has been carried out employing both the $N = 3$ and $N = 6$ values in the XP-PCM calculations, as in Table 3.

Since the SF_6 molecular crystal undergoes phase transitions with pressure,²³ an appropriate tuning of the N parameter allows to follow correctly the structural behavior in different pressure ranges, as it can be appreciated in Figure 4 where both computed and experimental Murnaghan²⁷ equations of state are reported. The computed Murnaghan equation of state with $N = 3$ closely resemble the experimental one for phase I,

Table 5. Calculated Frequencies (in cm^{-1}) at the Different Pressure Values (GPa) with Parameter $N = 3$

symmetry	0.0	0.7	1.9	2.8	3.9	5.4	7.4	10.2
T_{2u}	346.9	348.4	350.9	352.9	355.7	359.2	364.2	371.2
T_{2g}	517.5	518.6	520.8	522.3	524.6	527.3	531.5	537.7
T_{1u}	611.3	611.7	612.8	613.6	615.0	616.5	619.1	622.8
E_g	662.4	663.3	665.5	666.5	668.8	671.4	675.7	682.1
A_{1g}	771.2	772.6	775.5	777.1	780.0	783.0	788.0	795.7
T_{1u}	978.5	977.3	977.2	976.7	977.5	978.0	980.2	985.1

Table 6. Calculated Frequencies at the Different Pressure Values (GPa) with Parameter $N = 6$

symmetry	0.0	1.0	3.0	4.6	7.0	10.6	16.0	24.6
T_{2u}	346.9	348.7	352.4	355.6	360.6	367.2	377.0	391.6
T_{2g}	517.5	518.8	521.9	524.5	528.7	534.0	542.3	555.3
T_{1u}	611.3	611.9	613.8	615.3	618.0	621.5	627.1	635.6
E_g	662.4	663.6	667.0	669.3	673.7	679.3	688.5	702.8
A_{1g}	771.2	772.9	777.2	779.7	785.0	791.2	801.1	817.3
T_{1u}	978.5	977.6	978.6	979.1	982.2	985.4	992.3	1005.8

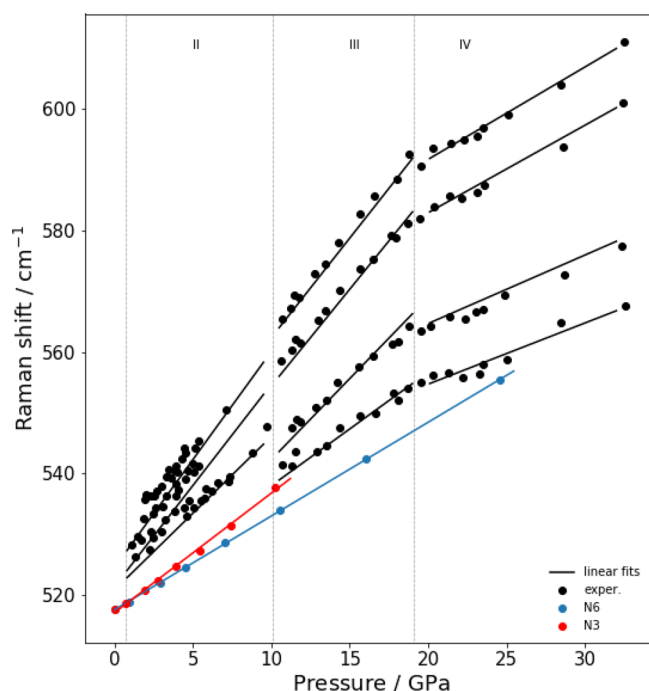


Figure 6. Experimental and computed vibrational frequencies of normal mode $\nu_5(T_{2g})$. The XP-PCM calculations have been carried out with both $N = 3$ and $N = 6$. The experimental data have been taken by Rademacher et al.²³

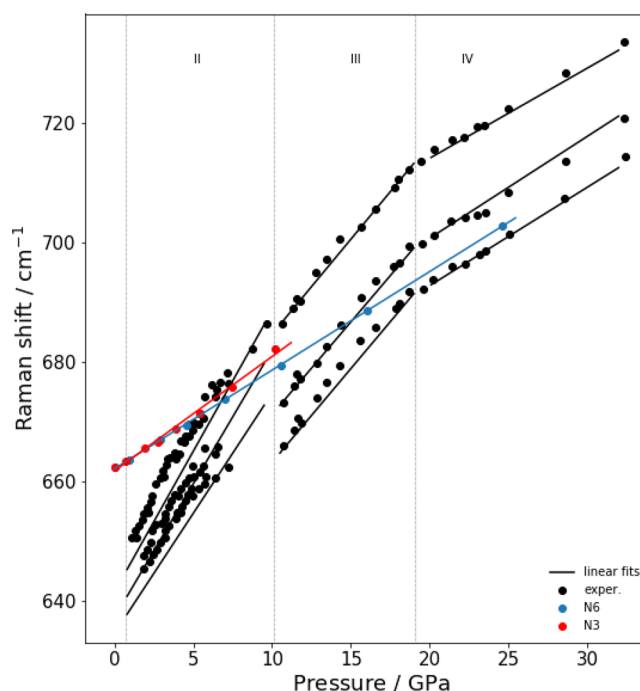


Figure 7. Experimental and computed vibrational frequencies of normal mode $\nu_2(E_g)$. The XP-PCM calculations have been carried out with both $N = 3$ and $N = 6$. The experimental data have been taken by Rademacher et al.²³

whereas the XP-PCM calculations with $N = 6$ reproduce the behavior of phase II.

Pressure Effects on Bond Lengths. The different effect due to the N parameter with increasing pressure provides further information on the compressibility of SF_6 . It is interesting to note (see Figure 5) that $N = 3$ and $N = 6$ parameters present a similar behavior for low pressure values, whereas a marked difference occurs for higher values, as confirmed by linear regression analysis. In fact, the correlation coefficients for the linear regression equations for PBE are $R^2 = 0.9907$ and $R^2 = 0.9870$ for $N = 3$ and $N = 6$, respectively, while the same coefficients for PBE0 are $R^2 = 0.9923$ and $R^2 = 0.9989$. By comparing the results obtained with both the PBE0 and PBE exchange and correlation functionals, it is possible to note that hybrid functionals provide a better agreement than GGA functionals with the experimental bond length³⁸ and a similar trend with pressure. The bond length contraction has the same order of magnitude, but it presents a slightly underestimated value.²³ Although marked volume variations are observed with the choice of N parameter as shown in Figure 3, the variation of the bond lengths are less affected by the N value. This behavior reflects on the calculated frequencies which are usually more accurate with PBE0 than PBE. This result further suggests to use hybrid functionals in

simulation of structural and vibrational properties by performing calculations with the XP-PCM method.

As previously observed in studying other systems with the XP-PCM method,^{4,13,16,17} the effect of pressure on SF_6 molecular structure can be analyzed considering eq 8. In fact, the variation of molecular structure with pressure are related both to pressure coupling coefficient Γ_i and to the stiffness of the normal modes. This analysis can be carried out through two different approaches. In the first case, the pressure coupling Γ_i (defined in eq 7) is estimated by a linear fitting of the nuclear gradient of G_{er} as function of pressure evaluated at the equilibrium geometry of the isolated molecule. The force constant k_i is determined from the calculation of the harmonic frequencies of the isolated molecule. In the second case, the linear coefficient ($\frac{dQ_i^{\text{eq}}}{dp}$) has been obtained by the projection of the atomic displacement on the eigenvector of the totally symmetric normal mode, as function of pressure. The two procedures have been performed for $N = 3$ and $N = 6$, and the final results, collected in Table 4, allow to verify eq 8.

Pressure Effects on the Vibrational Modes. The pressure effects on the vibrational frequencies have been obtained from calculations for the SF_6 pressure optimized geometrical structures (scaling factor, f) for both the $N = 3$ and

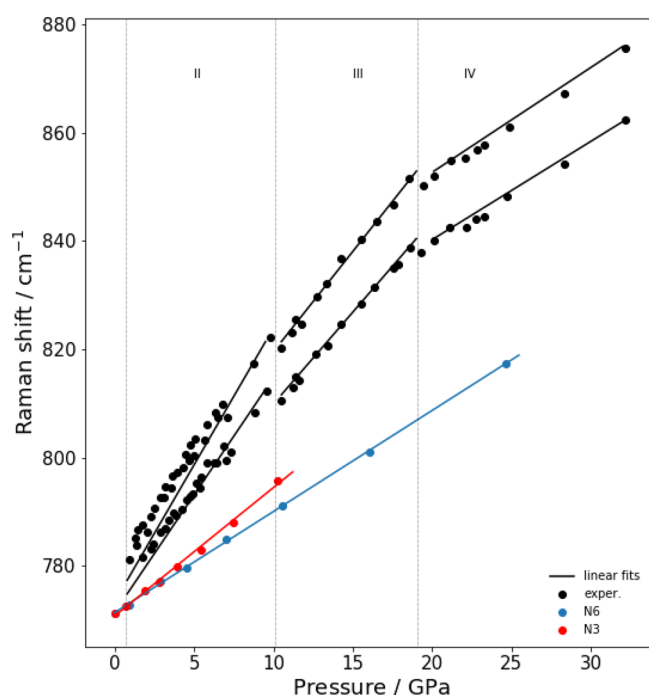


Figure 8. Experimental and computed vibrational frequencies of normal mode $\nu_1(A_{1g})$. The XP-PCM calculations have been carried out with both $N = 3$ and $N = 6$. The experimental data have been taken by Rademacher et al.²³

$N = 6$ parameters. The vibrational frequencies of the computed normal modes of SF_6 as a function of pressure are collected in Table 5 and 6.

Comparison with Experiments. The experimental trend of vibrational frequencies of the T_{2g} , E_g , and A_{1g} modes as a function of pressure is compared with calculations in Figure 6, Figure 7, and Figure 8, respectively. The experimental data refer the measurement results for phases II, III, and IV, while it has not been reported the vibrational frequencies relative to phase I.

The pressure effect on vibrational frequencies has been analyzed by the numerical calculation of the frequency slope, $\left(\frac{d\nu}{dp}\right)$, which differs for the various normal modes as found experimentally.²³ The model depends by the choice of N parameter as discussed above. However, either N parameters provide a semiquantitative description of the experimental data, also if the computed values underestimate the experimental results, as can be appreciated in Table 7. A similar behavior has been obtained in studying C_{60} and C_{70} fullerenes under pressure.¹⁶

Analysis of Pressure Effects on the Vibrational Frequencies. In this section we present a detailed analysis of the vibrational frequencies as a function of pressure in terms of

Table 8. Variations of Vibrational Frequencies (in cm^{-1}) with Pressure (GPa) for $N = 3$ and $N = 6$ Parameters^a

freq	symm	\tilde{g}_{ij}	$N = 3$			
			$\left(\frac{d\nu(p)}{dp}\right)_{Q(p)}$	$\left(\frac{d\nu}{dp}\right)_{\text{rel}}^{\text{num}}$	$\left(\frac{d\nu}{dp}\right)_{\text{rel}}^{\text{anal}}$	$\left(\frac{d\nu}{dp}\right)_{\text{cur}}$
346.9	T_{2u}	−10.5	2.39	−0.19	0.18	2.58
517.5	T_{2g}	−34.5	1.98	0.38	0.59	1.59
611.3	T_{1u}	−37.0	1.14	0.5	0.64	0.63
662.4	E_g	−76.5	1.92	1.22	1.31	0.70
771.2	A_{1g}	−98.5	2.38	1.62	1.70	0.76
978.5	T_{1u}	−108.5	0.65	2.15	1.87	−1.50

freq	symm	\tilde{g}_{ij}	$N = 6$			
			$\left(\frac{d\nu(p)}{dp}\right)_{Q(p)}$	$\left(\frac{d\nu}{dp}\right)_{\text{rel}}^{\text{num}}$	$\left(\frac{d\nu}{dp}\right)_{\text{rel}}^{\text{anal}}$	$\left(\frac{d\nu}{dp}\right)_{\text{cur}}$
346.9	T_{2u}	−10.5	1.83	−0.12	0.15	1.95
517.5	T_{2g}	−34.5	1.55	0.31	0.47	1.24
611.3	T_{1u}	−37.0	1.00	0.37	0.50	0.63
662.4	E_g	−76.5	1.65	0.96	1.04	0.70
771.2	A_{1g}	−98.5	1.87	1.29	1.35	0.58
978.5	T_{1u}	−108.5	1.14	1.61	1.48	−0.47

^aFreq and symm refer to normal mode frequencies (in cm^{-1}) and symmetries, respectively. \tilde{g}_{ij} represents the cubic force constant (in cm^{-1}). *cur* and *rel* subscripts indicate the curvature and relaxation terms, while *anal* and *num* superscripts refer to the calculation approaches.

curvature (direct) and relaxation (indirect) contributions, as given from eq 11 to eq 13. The curvature contribution has been obtained by calculating the vibrational frequencies of SF_6 keeping the geometry fixed to that of the isolated molecule but reducing the cavity volume to increase the pressure. The $\left(\frac{d\nu}{dp}\right)_{\text{cur}}$ term has been subsequently obtained through a fitting procedure of the vibrational frequencies, which have been reported in Table 8.

The relaxation contribution has been obtained by both the numeric and analytic approaches, described in “Computational Protocol and Details” section. The results with $N = 3$ and $N = 6$ are summarized in Table 8, while a graphic representation is shown in Figure 9.

The results of the vibrational frequency analysis can be summarized considering both the relaxation and curvature contributions. Independent of the value of N parameter, the relaxation term, $\left(\frac{d\nu}{dp}\right)_{\text{rel}}$, computed with both numerical and analytic approaches, grows with frequency of the normal modes at the expenses of the curvature term. The results obtained with either approaches, are similar and show that the $\left(\frac{d\nu}{dp}\right)_{\text{rel}}^{\text{num}}$ is positive with the exception of the lower frequency normal mode with symmetry T_{2u} . The same value is found for

Table 7. Comparison between Computed (for $N = 3$ and $N = 6$) and Experimental $\left(\frac{d\nu}{dp}\right)$ in $\frac{\text{cm}^{-1}}{\text{GPa}}$ ^a

freq	symm	$N = 3$	$N = 6$	phase II	phase III	phase IV
517.5	T_{2g}	1.98	1.55	2.73 ± 0.47	2.17 ± 0.61	1.18 ± 0.22
662.4	E_g	1.92	1.65	3.83 ± 0.31	3.13 ± 0.04	1.58 ± 0.08
771.2	A_{1g}	2.38	1.87	4.64 ± 0.33	3.55 ± 0.22	1.86 ± 0.08

^aThe experimental data refer to Raman measurements by Rademacher et al.²³ for the different SF_6 phases at high pressure.

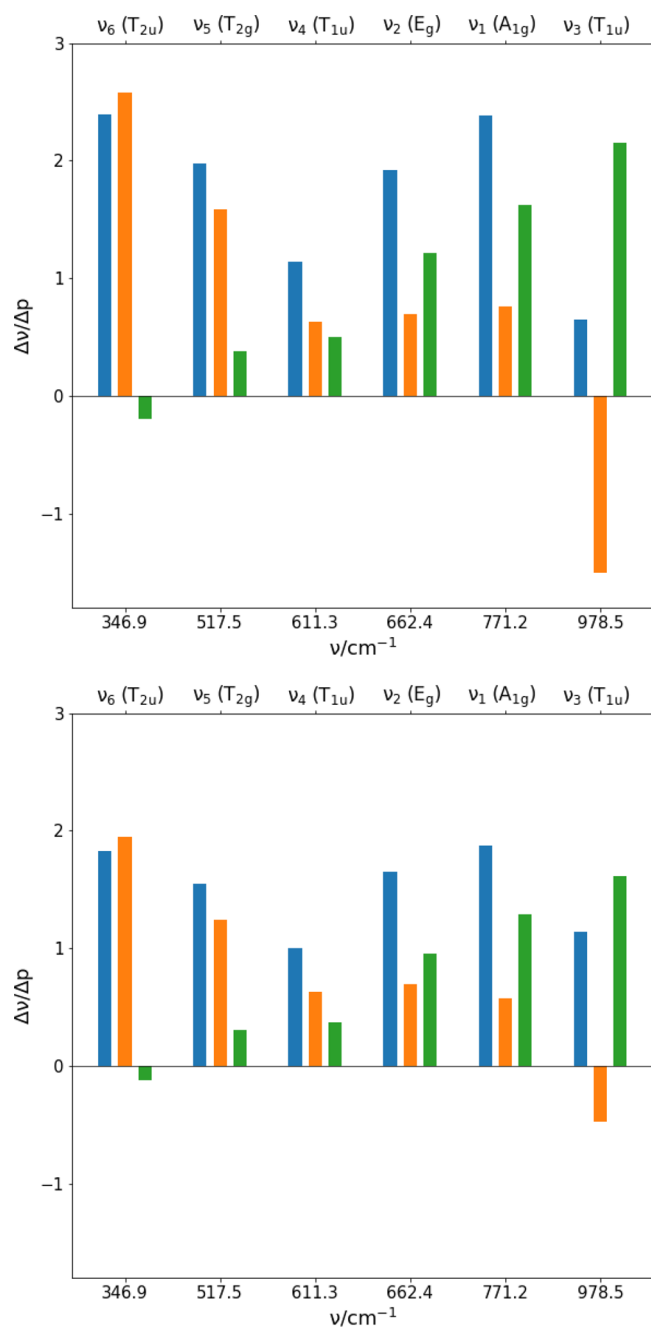


Figure 9. Vibrational analysis in terms of curvature (orange) and relaxation (green) contribution to $\left(\frac{d\nu}{dp}\right)$ (blue). The upper panel refers to the results obtained with $N = 3$, while the lower panel refers to the results obtained with $N = 6$.

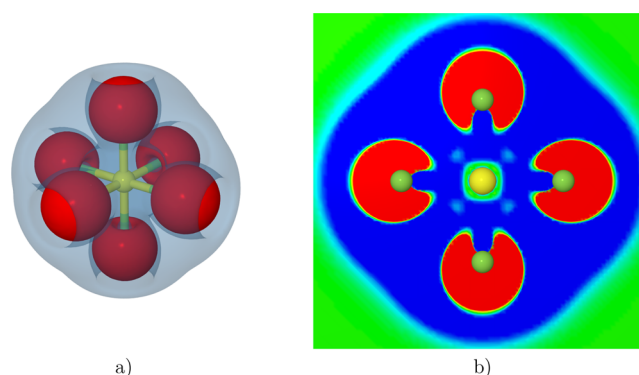


Figure 10. a) Electron density difference between SF_6 at 0.0 and 24.6 GPa (cutoff $\pm 3 \times 10^{-5}$). b) The red and blue colors on the map represent regions with increase and decrease of electron density, respectively. The isosurface cutoff is $\pm 1.5 \times 10^{-5}$.

$\left(\frac{d\nu}{dp}\right)_{\text{rel}}^{\text{anal}}$; it can only be noted that for $N = 6$ the value for T_{2u} mode is negative, but very small. In particular, the relaxation term is related to the anharmonicity through the cubic force constants as discussed in eq 13. In particular, the SF_6 molecule has only one totally symmetric normal mode (ν_1 of Figure 2), consequently the relaxation contribution has to be ascribed to the cubic anharmonic constants g_{ijj} in eq 13; the anharmonic constants g_{ijj} are reported in Table 8. The anharmonic character of the normal modes is more pronounced for the higher than for the lower frequency modes and it is more pronounced for stretching modes. This increasing of the anharmonicity is the origin of the growth of the relaxation term with frequencies.

The curvature term, $\left(\frac{d\nu}{dp}\right)_{\text{cur}}$, shows positive values with the exception of the highest frequency mode (ν_3) with symmetry T_{1u} . While the positive values of curvature term present a behavior similar to that found in other systems,^{16,17} the negative value of ν_3 is rather unusual. The behavior of ν_3 with pressure has been rationalized considering the Pauli repulsion due to pressure on the electronic structure of SF_6 , especially in the region along the S–F bond. The electron density variation has been analyzed in terms of Mayer bond order,^{57,58} atomic charges,^{59–63} and maps of the electron density difference. The different methods concord in the observed results. In fact, the Mayer bond order decreases with pressure from 0.907 to 0.893 going from 0 to 24.6 GPa with a difference of 0.014; the charges on fluorine atoms increase while that of sulfur decreases (independently by the method, as summarized in Table 9). These results confirm an increase in ionic character of the bond. A similar result has been obtained by the difference of electron density maps depicted in Figure 10. This

Table 9. S and F Atomic Charges (e) Computed through Mulliken,^{59–61} Löwdin,⁶² and Hirshfeld⁶³ Partition Schemes^a

	S			F		
	0.0 GPa	24.6 GPa	Δ	0.0 GPa	24.6 GPa	Δ
Mulliken	1.576	1.617	−0.041	−0.263	−0.270	0.007
Löwdin	1.285	1.303	−0.018	−0.214	−0.217	0.003
Hirshfeld	0.598	0.604	−0.006	−0.100	−0.101	0.001

^aThe differences on atomic charges (Δ) of both S and F atoms have been computed considering the system at the pressure values of 0.0 and 24.6 GPa.

behavior substantially differs from that found in studying other systems,^{13,16,17} which show an increase of electron density on the bond regions. In the case of SF₆, the observed electron structure rearrangement with pressure induces a more pronounced variation in the normal modes with asymmetric displacement with respect to the S–F bond.

CONCLUSIONS

The XP-PCM method has been applied to compute the structural and vibrational properties of SF₆ with pressure. The results of the XP-PCM method have been compared with both structural and spectroscopic experimental data, showing a reasonable agreement between experiments and calculations. Pressure effects on the vibrational frequencies have been analyzed by considering both the contribution of curvature, $\left(\frac{d\nu}{dp}\right)_{\text{cur}}$, and relaxation, $\left(\frac{d\nu}{dp}\right)_{\text{rel}}$, obtaining useful information for discriminating the importance of confinement and anharmonicity effects. In particular, the curvature term for the ν_3 normal modes has been rationalized considering the variation of electronic structure of SF₆ with pressure. In fact, it has been observed that this behavior can be related to the increase of ionic character of the S–F bond under pressure. These results show how the XP-PCM method could provide further useful information for the interpretation of the experimental findings. The different pressure effects in determining a more pronounced covalent or ionic character of bonds in a molecule represent an interesting point to be analyzed in more detail to rationalize the trend of vibrational frequencies with pressure not only using the XP-PCM method but other single molecule computational approaches.^{6,64–69} Finally, it would be useful to extend this kind of analysis in periodic DFT calculations on molecular crystalline systems, which explicitly describe the intermolecular interactions to achieve further information on spectroscopic properties.

AUTHOR INFORMATION

Corresponding Authors

Roberto Cammi – Dipartimento di Scienze Chimiche, della Vita e della Sostenibilità Ambientale, Università degli Studi di Parma, 43124 Parma, Italy; orcid.org/0000-0002-7026-7750; Email: roberto.cammi@unipr.it

Marco Pagliai – Dipartimento di Chimica “Ugo Schiff”, Università degli Studi di Firenze, 50019 Sesto Fiorentino, Italy; orcid.org/0000-0003-0240-161X; Email: marco.pagliai@unifi.it

Gianni Cardini – Dipartimento di Chimica “Ugo Schiff”, Università degli Studi di Firenze, 50019 Sesto Fiorentino, Italy; orcid.org/0000-0002-7292-3555; Email: gianni.cardini@unifi.it

Authors

Matteo Boccalini – Dipartimento di Chimica “Ugo Schiff”, Università degli Studi di Firenze, 50019 Sesto Fiorentino, Italy; orcid.org/0000-0002-6392-4978

Vincenzo Schettino – Dipartimento di Chimica “Ugo Schiff”, Università degli Studi di Firenze, 50019 Sesto Fiorentino, Italy

Complete contact information is available at:
<https://pubs.acs.org/10.1021/acs.jpca.1c02595>

Notes

The authors declare no competing financial interest.

ACKNOWLEDGMENTS

The authors (M.B., M.P., G.C., and V.S.) thank MIUR-Italy (“Progetto Dipartimenti di Eccellenza 2018-2022” allocated to Department of Chemistry “Ugo Schiff”). R.C. is thankful for support the framework of the COMP-HUB Initiative of the Department of Chemistry, Life Sciences and Environmental Sustainability of the University of Parma, as part of the ‘Departments of Excellence’ program of the Italian Ministry for Education, University and Research (MIUR, 2018-2022).

REFERENCES

- (1) Schettino, V.; Bini, R. Constraining Molecules at the Closest Approach: Chemistry at High Pressure. *Chem. Soc. Rev.* **2007**, *36*, 869–880.
- (2) Bini, R.; Schettino, V. *Materials Under Extreme Conditions*; Imperial College Press, 2014.
- (3) Li, B.; Ji, C.; Yang, W.; Wang, J.; Yang, K.; Xu, R.; Liu, W.; Cai, Z.; Chen, J.; Mao, H.-k. Diamond anvil cell behavior up to 4 Mbar. *Proc. Natl. Acad. Sci. U. S. A.* **2018**, *115*, 1713–1717.
- (4) Cammi, R. In *Frontiers of Quantum Chemistry*; Wójcik, M. J., Nakatsuji, H., Kirtman, B., Ozaki, Y., Eds.; Springer Singapore: Singapore, 2018; pp 273–287.
- (5) Grochala, W.; Hoffmann, R.; Feng, J.; Ashcroft, N. The Chemical Imagination at Work in Very Tight Places. *Angew. Chem., Int. Ed.* **2007**, *46*, 3620–3642.
- (6) Stauch, T. Quantum chemical modeling of molecules under pressure. *Int. J. Quantum Chem.* **2021**, *121*, e26208.
- (7) Chen, B.; Hoffmann, R.; Cammi, R. The Effect of Pressure on Organic Reactions in Fluids—a New Theoretical Perspective. *Angew. Chem., Int. Ed.* **2017**, *56*, 11126–11142.
- (8) Cammi, R.; Rahm, M.; Hoffmann, R.; Ashcroft, N. W. Varying Electronic Configurations in Compressed Atoms: From the Role of the Spatial Extension of Atomic Orbitals to the Change of Electronic Configuration as an Isobaric Transformation. *J. Chem. Theory Comput.* **2020**, *16*, 5047–5056.
- (9) Califano, S.; Schettino, V.; Neto, N. *Lattice Dynamics of Molecular Crystals*; Springer: Berlin, Heidelberg, 1981.
- (10) Martin, R. M. *Electronic Structure: Basic Theory and Practical Methods*; Cambridge University Press, 2004.
- (11) Marx, D.; Hutter, J. *Ab Initio Molecular Dynamics: Basic Theory and Advanced Methods*; Cambridge University Press, 2009.
- (12) Wang, Y.; Shang, S.-L.; Fang, H.; Liu, Z.-K.; Chen, L.-Q. First-principles calculations of lattice dynamics and thermal properties of polar solids. *npj Comput. Mater.* **2016**, *2*, 16006.
- (13) Cammi, R.; Cappelli, C.; Mennucci, B.; Tomasi, J. Calculation and analysis of the harmonic vibrational frequencies in molecules at extreme pressure: Methodology and diborane as a test case. *J. Chem. Phys.* **2012**, *137*, 154112.
- (14) Fukuda, R.; Ehara, M.; Cammi, R. Modeling Molecular Systems at Extreme Pressure by an Extension of the Polarizable Continuum Model (PCM) Based on the Symmetry-Adapted Cluster-Configuration Interaction (SACCI) Method: Confined Electronic Excited States of Furan as a Test Case. *J. Chem. Theory Comput.* **2015**, *11*, 2063–2076.
- (15) Cammi, R. A new extension of the polarizable continuum model: Toward a quantum chemical description of chemical reactions at extreme high pressure. *J. Comput. Chem.* **2015**, *36*, 2246–2259.
- (16) Pagliai, M.; Cardini, G.; Cammi, R. Vibrational frequencies of fullerenes C60 and C70 under pressure studied with a quantum chemical model including spatial confinement effects. *J. Phys. Chem. A* **2014**, *118*, 5098–5111.
- (17) Pagliai, M.; Cammi, R.; Cardini, G.; Schettino, V. XP-PCM Calculations of High Pressure Structural and Vibrational Properties of P₄S₃. *J. Phys. Chem. A* **2016**, *120*, 5136–5144.

- (18) Caratelli, C.; Cammi, R.; Chelli, R.; Pagliai, M.; Cardini, G.; Schettino, V. Insights on the Realgar Crystal Under Pressure from XP-PCM and Periodic Model Calculations. *J. Phys. Chem. A* **2017**, *121*, 8825–8834.
- (19) Tomasi, J.; Persico, M. Molecular Interactions in Solution: An Overview of Methods Based on Continuous Distributions of the Solvent. *Chem. Rev.* **1994**, *94*, 2027–2094.
- (20) Tomasi, J.; Mennucci, B.; Cammi, R. Quantum Mechanical Continuum Solvation Models. *Chem. Rev.* **2005**, *105*, 2999–3094.
- (21) Labet, V.; Hoffmann, R.; Ashcroft, N. W. A Fresh Look at Dense Hydrogen under Pressure. II. Chemical and Physical Models Aiding our Understanding of Evolving H-H Separations. *J. Chem. Phys.* **2012**, *136*, 074502.
- (22) Salvi, P.; Schettino, V. Infrared and Raman spectra and phase transition of the SF₆ crystal. Anharmonic interactions and two-phonon infrared absorption. *Chem. Phys.* **1979**, *40*, 413–424.
- (23) Rademacher, N.; Friedrich, A.; Morgenroth, W.; Bayarjargal, L.; Milman, V.; Winkler, B. High-pressure phases of SF₆ up to 32 GPa from X-ray diffraction and Raman spectroscopy. *J. Phys. Chem. Solids* **2015**, *80*, 11–21.
- (24) Dows, D. A.; Wieder, G. M. Infrared intensities in crystalline SF₆. *Spectrochim. Acta* **1962**, *18*, 1567–1574.
- (25) Rubin, B.; McCubbin, T.K.; Polo, S.R. Vibrational Raman Spectrum of SF₆. *J. Mol. Spectrosc.* **1978**, *69*, 254–259.
- (26) Sasaki, S.; Tomida, Y.; Shimizu, H. High-Pressure Raman Study of Sulfur Hexafluoride up to 10 GPa. *J. Phys. Soc. Jpn.* **1992**, *61*, 514–518.
- (27) Murnaghan, F. D. The Compressibility of Media under Extreme Pressures. *Proc. Natl. Acad. Sci. U. S. A.* **1944**, *30*, 244–247.
- (28) Alvarez, S. A cartography of the van der Waals territories. *Dalton Trans.* **2013**, *42*, 8617–8636.
- (29) Rahm, M.; Ångqvist, M.; Rahm, J. M.; Erhart, P.; Cammi, R. Non-Bonded Radii of the Atoms Under Compression. *ChemPhysChem* **2020**, *21*, 2441–2453.
- (30) Moroni, L.; Ceppatelli, M.; Gellini, C.; Salvi, P. R.; Bini, R. Excitation of Crystalline All Trans Retinal under Pressure. *Phys. Chem. Chem. Phys.* **2002**, *4*, 5761–5767.
- (31) Cockcroft, J. K.; Fitch, A. N. The solid phases of sulphur hexafluoride by powder neutron diffraction. *Z. Kristallogr.* **1988**, *184*, 123–145.
- (32) Dolling, G.; Powell, B.; Sears, V. Neutron diffraction study of the plastic phases of polycrystalline SF₆ and CBr₄. *Mol. Phys.* **1979**, *37*, 1859–1883.
- (33) Dove, M. T.; Pawley, G. S. A molecular dynamics simulation study of the plastic crystalline phase of sulphur hexafluoride. *J. Phys. C: Solid State Phys.* **1983**, *16*, 5969–5983.
- (34) Dove, M. T.; Pawley, G. S. A molecular dynamics simulation study of the orientationally disordered phase of sulphur hexafluoride. *J. Phys. C: Solid State Phys.* **1984**, *17*, 6581–6599.
- (35) Dove, M.; Tucker, M.; Keen, D. Neutron total scattering method: simultaneous determination of long-range and short-range order in disordered materials. *Eur. J. Mineral.* **2002**, *14*, 331–348.
- (36) Spitznagel, G. W.; Clark, T.; Schleyer, P. v.; Hehre, W. J. An Evaluation of the Performance of Diffuse Function-Augmented Basis Sets for Second Row Elements, Na-Cl. *J. Comput. Chem.* **1987**, *8*, 1109–1116.
- (37) Frisch, M. J.; Trucks, G. W.; Schlegel, H. B.; Scuseria, G. E.; Robb, M. A.; Cheeseman, J. R.; Scalmani, G.; Barone, V.; Mennucci, B.; Petersson, G. A.; et al. *Gaussian'09 Revision C.01*; Gaussian Inc.: Wallingford, CT, 2010.
- (38) Bartell, L.; Doun, S. Structures of hexacoordinate compounds of main-group elements: Part III. An electron diffraction study of SF₆. *J. Mol. Struct.* **1978**, *43*, 245–249.
- (39) Hohenberg, P.; Kohn, W. Inhomogeneous Electron Gas. *Phys. Rev.* **1964**, *136*, B864–B871.
- (40) Kohn, W.; Sham, L. J. Self-Consistent Equations Including Exchange and Correlation Effects. *Phys. Rev.* **1965**, *140*, A1133–A1138.
- (41) Slater, J. C. *The Self-Consistent Field for Molecular and Solids, Quantum Theory of Molecular and Solids*; McGraw-Hill: New York, 1974; Vol. 4.
- (42) Vosko, S. H.; Wilk, L.; Nusair, M. Accurate spin-dependent electron liquid correlation energies for local spin density calculations: a critical analysis. *Can. J. Phys.* **1980**, *58*, 1200–1211.
- (43) Becke, A. D. Density-functional exchange-energy approximation with correct asymptotic behavior. *Phys. Rev. A: At., Mol., Opt. Phys.* **1988**, *38*, 3098–3100.
- (44) Lee, C.; Yang, W.; Parr, R. Development of the Colle-Salvetti Correlation-Energy Formula into a Functional of the Electron-Density. *Phys. Rev. B: Condens. Matter Mater. Phys.* **1988**, *37*, 785–789.
- (45) Becke, A. D. Density-Functional Thermochemistry. III. The Role of Exact Exchange. *J. Chem. Phys.* **1993**, *98*, 5648–5652.
- (46) Yanai, T.; Tew, D. P.; Handy, N. C. A new hybrid exchange-correlation functional using the Coulomb-attenuating method (CAM-B3LYP). *Chem. Phys. Lett.* **2004**, *393*, 51–57.
- (47) Cohen, A. J.; Handy, N. C. Dynamic correlation. *Mol. Phys.* **2001**, *99*, 607–615.
- (48) Perdew, J. P.; Burke, K.; Ernzerhof, M. Generalized Gradient Approximation Made Simple. *Phys. Rev. Lett.* **1996**, *77*, 3865–3868.
- (49) Perdew, J. P.; Burke, K.; Ernzerhof, M. Generalized Gradient Approximation Made Simple [Phys. Rev. Lett. *77*, 3865 (1996)]. *Phys. Rev. Lett.* **1997**, *78*, 1396–1396.
- (50) Adamo, C.; Barone, V. Toward Reliable Density Functional Methods without Adjustable Parameters: The PBE0 Model. *J. Chem. Phys.* **1999**, *110*, 6158–6169.
- (51) Chai, J.-D.; Head-Gordon, M. Long-range corrected hybrid density functionals with damped atom-atom dispersion corrections. *Phys. Chem. Chem. Phys.* **2008**, *10*, 6615–6620.
- (52) Cammi, R.; Verdolino, V.; Mennucci, B.; Tomasi, J. Towards the Elaboration of a QM Method to Describe Molecular Solutes under Effect of a Very High Pressure. *Chem. Phys.* **2008**, *344*, 135–141.
- (53) Herzberg, G. *Molecular Spectra and Molecular Structure II. Infrared and Raman Spectra of Polyatomic Molecules*; Krieger: Malabar, FL, 1991.
- (54) Edelson, D.; McAfee, K. Note on the infrared spectrum of sulfur hexafluoride. *J. Chem. Phys.* **1951**, *19*, 1311–1312.
- (55) Wagner, N. L.; Wüest, A.; Christov, I. P.; Popmitchnev, T.; Zhou, X.; Murnane, M. M.; Kapteyn, H. C. Monitoring molecular dynamics using coherent electrons from high harmonic generation. *Proc. Natl. Acad. Sci. U. S. A.* **2006**, *103*, 13279–13285.
- (56) Birch, F. Finite Elastic Strain of Cubic Crystals. *Phys. Rev.* **1947**, *71*, 809–824.
- (57) Mayer, I. Charge bond order and valence in the AB initio SCF theory. *Chem. Phys. Lett.* **1983**, *97*, 270–274.
- (58) Mayer, I. On bond orders and valences in the Ab initio quantum chemical theory. *Int. J. Quantum Chem.* **1986**, *29*, 73–84.
- (59) Mulliken, R. S. Electronic Population Analysis on LCAO-MO Molecular Wave Functions. I. *J. Chem. Phys.* **1955**, *23*, 1833–1840.
- (60) Mulliken, R. S. Electronic Population Analysis on LCAOMO Molecular Wave Functions. II. Overlap Populations, Bond Orders, and Covalent Bond Energies. *J. Chem. Phys.* **1955**, *23*, 1841–1846.
- (61) Mulliken, R. S. Criteria for the Construction of Good Self-Consistent-Field Molecular Orbital Wave Functions, and the Significance of LCAO-MO Population Analysis. *J. Chem. Phys.* **1962**, *36*, 3428–3439.
- (62) Löwdin, Per-Olov On the Non-Orthogonality Problem Connected with the Use of Atomic Wave Functions in the Theory of Molecules and Crystals. *J. Chem. Phys.* **1950**, *18*, 365–375.
- (63) Hirshfeld, F. Bonded-atom fragments for describing molecular charge densities. *Theoret. Chim. Acta* **1977**, *44*, 129–138.
- (64) Subramanian, G.; Mathew, N.; Leiding, J. A generalized force-modified potential energy surface for mechanochemical simulations. *J. Chem. Phys.* **2015**, *143*, 134109.
- (65) Zaleśny, R.; Góra, R. W.; Luis, J. M.; Bartkowiak, W. On the particular importance of vibrational contributions to the static

electrical properties of model linear molecules under spatial confinement. *Phys. Chem. Chem. Phys.* **2015**, *17*, 21782–21786.

(66) Spooner, J.; Smith, B.; Weinberg, N. Effect of high pressure on the topography of potential energy surfaces. *Can. J. Chem.* **2016**, *94*, 1057–1064.

(67) Stauch, T. A mechanochemical model for the simulation of molecules and molecular crystals under hydrostatic pressure. *J. Chem. Phys.* **2020**, *153*, 134503.

(68) Chouj, M.; Basiak, B.; Bartkowiak, W. Partitioning of the interaction-induced polarizability of molecules in helium environments. *Int. J. Quantum Chem.* **2021**, *121*, e26544.

(69) Scheurer, M.; Dreuw, A.; Epifanovsky, E.; Head-Gordon, M.; Stauch, T. Modeling Molecules under Pressure with Gaussian Potentials. *J. Chem. Theory Comput.* **2021**, *17*, 583–597.